Astron. Astrophys. 323, 953–962 (1997)

ASTRONOMY
AND
ASTROPHYSICS

Physical models of photon-dominated regions: influence of clumpiness and geometry for S 140

Marco Spaans[1] **and Ewine F. van Dishoeck**[2]

[1]Johns Hopkins University, Bloomberg, 3400 N. Charles St., Baltimore, MD 21218, USA
[2]Sterrewacht Leiden, P.O. Box 9513, 2300 RA Leiden, The Netherlands

Received 14 August 1996 / Accepted 14 January 1997

Abstract. Model calculations for the photon-dominated region S 140 are presented. The overall geometry and an inhomogeneous density distribution are incorporated and the chemical and thermal balance is solved in two and three dimensions. The observed widespread neutral carbon emission in the extended molecular cloud is investigated for a range in clump size and volume filling factor. It is found that the clump volume filling factor needs to be less than 30% and the clump size larger than 0.2 pc in order to reproduce the observed [CI] data and their correlation with ^{13}CO. Because of the presence of a dense core near the edge of the cloud, a large part of the stellar radiation cannot penetrate the extended molecular cloud. Therefore, to explain the [CI] extent, the star must be located closer to the sun, i.e. off the direction defined by the line center cloud – dense core. The dense core itself contains three embedded young stars, which influence the source morphology of the dense interface region. Detailed models including these internal sources are constructed and the results compare well with high spatial resolution observations.

Maps of the [C II], [C I], [O I] and CO line emission are presented for various cases, and their relation with the underlying geometry and density distribution is discussed. It is found that geometrical effects play a central role in the resulting intensity and morphology of line maps.

Key words: interstellar medium: clouds: individual S 140 – interstellar: molecules – radio lines

1. Introduction

In the last decade, Photon-Dominated Regions (PDRs) have received a lot of observational and theoretical attention. These clouds, which are exposed to intense far–ultraviolet radiation, contain warm regions in which hydrogen and carbon are being transformed from atomic to molecular form. PDRs are therefore bright emitters of submillimeter and far–infrared atomic and molecular lines. Recent advances in the technology at these wavelengths have made the widespread detection of e.g., the [CI] 609 μm line (Plume et al. 1994; Keene 1995; Tauber et al. 1995; Minchin et al. 1994), the [CII] 158 μm line (Boreiko et al. 1990; Stacey et al. 1993; Yui et al. 1993; Jaffe et al. 1994), the 7-6 and 6–5 lines of CO and its isotopes (Graf et al. 1990; Jansen et al. 1996) and vibrationally–excited H_2 pumped by ultraviolet photons (Luhman et al. 1994) possible from ground and space–based observatories.

Early models of PDRs considered a one–dimensional, homogeneous plane–parallel geometry (Tielens & Hollenbach 1985; Sternberg 1986; van Dishoeck & Black 1988; Burton et al. 1990; Hollenbach et al. 1991; Le Bourlot et al. 1993; Köster et al. 1994). Such models were remarkably successful in explaining many of the observed features of PDRs at the edges, such as the H→H_2 and C^+→CO chemical transitions, as well as the high gas temperatures generally found in PDRs. However, they failed to reproduce the early observations of extended emission of [CI] (Keene et al. 1985) and [CII] (Stutzki et al. 1988) deeper into clouds, as well as the intense ^{13}CO 6–5 emission in some regions (Graf et al. 1990). These data, together with large scale CO maps by, e.g., Falgarone & Pérault (1988), led to the suggestion that interstellar clouds have a very inhomogeneous structure, so that ultraviolet radiation can penetrate deeper into the cloud. Not only this "clumpy" structure, but also the overall geometry of the region can play a large role, as evidenced by recent observations of the Horsehead nebula and the Orion Bar (Zhou et al. 1993; Hogerheijde et al. 1995).

The first attempts to incorporate the effects of an inhomogeneous structure on the penetration of ultraviolet continuum radiation were made by Stutzki et al. (1988) and Boissé (1990). To compute the strengths of various atomic and molecular lines, Howe et al. (1991) and Meixner & Tielens (1993) used a more pragmatic approach, in which they superposed the results of homogeneous models with different densities, and used the average transparency of an inhomogeneous two–phase medium as tabulated by Boissé (1990). However, none of these models took

Send offprint requests to: M. Spaans

the line radiative transfer in an inhomogeneous model properly into account.

Spaans (1996) has recently presented a Monte Carlo method in which the radiative transfer in both the continuum and the ultraviolet lines through which the photodissociation of H_2 and CO occurs, can be modeled in a cloud with an arbitrary density structure and geometry. These models provide an accurate description of the self–shielding transition in both H_2 and CO, which is necessary for a good representation of the C and C^+ abundances throughout the region. Only through such maps is it possible to determine quantitatively the influence of the density structure and geometry on the abundances and excitation of the different species.

So far, the models of Spaans (1996) have mainly been used to illustrate the effects of a non–homogeneous density structure in a general sense, but comparison with observations of specific clouds has been limited. The importance of taking the actual geometry of the cloud into account has been demonstrated for the PDRs IC 63 (Jansen et al. 1995a) and the Orion Bar (Jansen et al. 1995b), but the need to include clumpiness has not been explored in detail. We present here models of the edge–on PDR S 140, which has been considered to be one of the clearest cases for an inhomogeneous structure.

The S 140 molecular cloud lies at a distance of $\sim$900 pc (Crampton & Fisher 1974) and is illuminated from the south–western side by the B0V star HD 211880. The star is located $\sim 7'$ (1.85 pc) from the edge of the cloud, at which position the enhancement of the radiation field is $I_{\rm UV} \approx$150. The cloud extends over more than $30'$ (8 pc) and contains a dense core in which star formation occurs, as evidenced by the presence of three embedded infrared sources (IRS1-3, Blair et al. 1978; Beichman et al. 1979). These embedded sources are young stars with spectral types of B1.5-B2 (Evans et al. 1989) which can illuminate the S 140 region from within.

For our purposes, we distinguish two different regions: (i) the extended molecular cloud, and (ii) the interface region near the south–west edge of the cloud, which also contains the star–formation core. A sketch of the region is given in Fig. 1. Keene et al. (1985), Hernichel et al. (1992) and Plume et al. (1994) have found [CI] emission throughout this cloud extending over nearly 10 pc, whereas White & Padman (1991) and Minchin et al. (1993, 1994) have obtained high resolution data of the interface region. The aim of this study is to compare our models with these and other observational data to provide quantitative constraints on the sizes and filling factors of the putative clumps, as well as the importance of the geometry of the region.

Sect. 2 summarizes the physical and chemical processes included in the models. Sect. 3 describes the physical characteristics of S 140 and the results of the model calculations for the extended molecular cloud, whereas Sect. 4 addresses the interface region. The conclusions and suggestions for further investigations are presented in Sect. 5.

2. Physical model

The inhomogeneous Monte Carlo code as described in Spaans (1996) is used to calculate the chemical structure and heat balance. The calculations for the S 140 interface region are two-dimensional, but those for the molecular cloud are also three-dimensional. The input parameters to the model are the density structure, the incident radiation field, and the geometry and total extent of the cloud. The density structure is characterized by the average density $< n_{\rm H} >$, the clump–interclump density ratio $R_{\rm ic}$, the volume filling factor of the clumps F and the size of the clumps $\ell_{\rm cl}$. The relation between the average density $< n_{\rm H} >$, the clump density n_h and the interclump density n_l is given by $< n_{\rm H} >= Fn_h + (1-F)n_l$ and $n_h = R_{\rm ic} n_l$. The location of the clumps is chosen to be random within the grid. A clump is represented as a sphere with a radius of five times the spatial resolution of the grid. Thus, the grid resolution determines the typical physical extent of the clumps $\ell_{\rm cl}$. No clump size hierarchy is assumed a priori, but adjacent clumps will lead to more extended structures.

It is assumed that the pressure in the clumps is dominated by turbulence according to a Gaussian velocity field with width δv_d = 3 km s^{-1}, $P = 0.5\rho\delta v_d^2$, where ρ is the mass density. Apart from a factor of 2 associated with the H/H_2 transition, the medium is therefore in (approximate) pressure equilibrium. In the presence of clumps, dynamical effects are likely to be important and the pressure equilibrium of the clumps should be computed rigorously. These putative clumpy structures are not self-gravitating and are likely to be transient objects. A full hydrodynamic treatment of this problem is beyond the scope of the present investigation, however.

The incident radiation field is expressed in units $I_{\rm UV}$ of the Draine (1978) average interstellar radiation field. The spectrum of this radiation field is characteristic of that of a B0–B1 star, and should therefore be appropriate for the B0V star HD 211880. At the edge of the cloud ($\sim 7'$ or 1.85 pc from the star), Keene et al. (1985) estimated that the enhancement is $I_{\rm UV} \approx 150$. Recently, Timmermann et al. (1996) used detailed non-LTE stellar atmosphere models to obtain a somewhat higher value of $I_{\rm UV}$ = 260. Because of the proximity of the star, the divergence of the incident radiation field is treated explicitly.

The chemical network adopted for the interface region includes 663 reactions between 116 species consisting of the elements hydrogen, deuterium, helium, carbon (^{12}C and ^{13}C with an isotopic ratio of 60), oxygen, silicon, sulfur, magnesium, iron, chlorine, and large molecules such as Polycyclic Aromatic Hydrocarbons (PAHs, with charges -1, 0, +1). Note that this chemical network is more extended than the one adopted in Spaans (1996). The current network is described in detail in Jansen et al. (1995a). For the extended molecular cloud, the 2–D calculations use the same network. In order to make the 3–D calculations feasible, however, a more restricted chemical network including 291 reactions between 51 species consisting of the elements hydrogen, carbon (^{12}C), oxygen, iron, magnesium, and PAHs (with charges -1, 0, and +1) was used. This network was

constructed to accurately model the C^+/C/CO transition, but not the rest of the chemistry.

The gas phase abundances of carbon, oxygen, iron and magnesium are taken to be A(C)=2.0 $\times$ 10^{-4}, A(O)=5.0 $\times$ 10^{-4}, A(Fe)=2.5 $\times$ 10^{-7} and A(Mg)=1.3 $\times$ 10^{-6}, respectively. For carbon this implies that about 50% of the solar abundance is present in the gas phase, which is comparable to the values found in diffuse clouds (Cardelli et al. 1993). It is assumed that 10% of the gas phase carbon is in the form of PAHs. The H_3^+ dissociative recombination rate has been taken equal to 8.0×10^{-7} $T^{-0.7}$ cm^3 s^{-1}, as suggested by the laboratory measurements of Smith & Spañel (1993). The cosmic ray ionization rate was set at $\zeta = 5 \times 10^{-17}$ s^{-1}.

The following mechanisms for converting the ultraviolet flux into gas heating have been included (see Spaans 1996 for details): (1) photo-electric emission from dust grains and large molecules like Polycyclic Aromatic Hydrocarbons (PAHs) (Bakes & Tielens 1994; Spaans et al. 1994), (2) neutral carbon ionization, (3) H_2 photodissociation, (4) FUV pumping followed by collisional de-excitation of vibrationally excited H_2 in the two level approximation, and (5) H_2 formation on grain surfaces. In addition, (6) cosmic-ray heating may also contribute deep into the cloud, and (7) OI may heat the gas through the collisional de-excitation of the $^3P_1$ fine structure level excited by (dust) continuum radiation.

For the cooling the infrared fine-structure lines from the atoms C, C^+, O, Si, and Fe, if present in the chemical network, have been taken into account. The lowest 20 rotational levels of CO are calculated in statistical equilibrium and their contribution to the cooling is included. H_2 rotational line cooling is considered as well, where the levels are assumed to be thermally excited and the lines optically thin. The adopted collision rates are given in Spaans et al. (1994, their Table 1).

The program calculates the gas and dust temperature, cooling and heating rates and the density and column density of atomic and molecular species as functions of position. The emergent intensities in the various atomic and molecular cooling lines are computed as well, taking into account optical depth effects and solving for the level populations in statistical equilibrium (Spaans 1996).

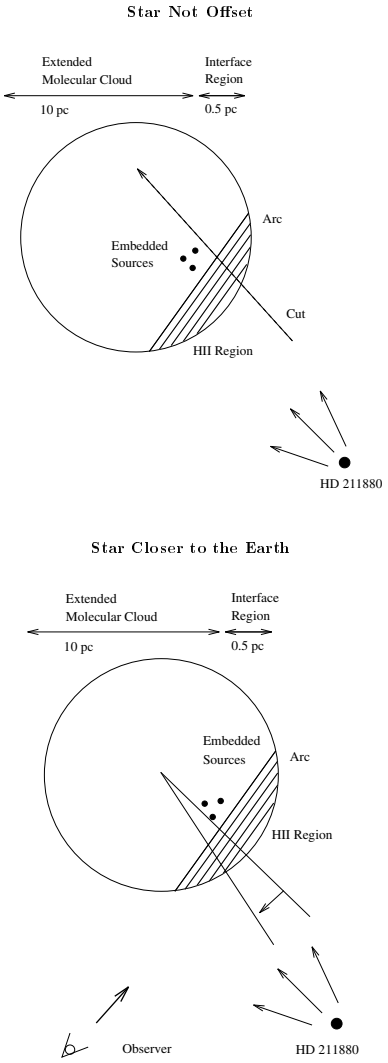

Fig. 1. Sketch of the adopted geometry for the S 140 interface region and extended molecular cloud. Figures are not to scale. The embedded sources are located in a dense core just next to the interface region. In Fig. 1a (upper panel) the observer is located above the paper. In Fig. 1b (lower panel) the illuminating star is moved closer to the sun through an angle of 10° with respect to the line through the dense core and the center of the molecular cloud.

3. The S 140 extended molecular cloud

Initial observations of [CI] and CO emission on a strip into the molecular cloud perpendicular to the ionization front by Keene et al. (1985) indicated that neutral carbon and ^{13}CO coexist to large depths. Recent large scale maps ($\sim$ 20$'$ $\times$ 30$'$) obtained by Plume et al. (1994) at 3$'$ resolution confirm this close correlation between the [CI] and ^{13}CO distribution out to at least 20$'$ (5 pc) from the south–west edge of the cloud. At this distance, the [CI] intensity is still at least 15% of its peak value of $\sim$16 K km s^{-1}. In homogeneous PDR models, the C abundance typically has dropped by a factor of four after 0.5 pc or 1 mag of extinction for $n_{\rm H}$ = 1000 cm^{-3}. As discussed above, several authors have suggested that the enhanced penetration is due to the inhomogeneous structure of the cloud (Stutzki et al. 1988; Howe et al. 1991 and references therein).

In order to obtain quantitative information on the degree of inhomogeneity (e.g., clump volume filling factor and clump size), a number of different models were calculated. The comparison with both the [C I] and the CO emission is important, since the former traces mostly the total surface area of the clumps, whereas the latter is more sensitive to the total volume of the clumps (Jaffe et al. 1994). The cloud is modeled as a sphere with a diameter of $\sim$ 10 pc. The star, the dense core, and the center of the molecular cloud are initially assumed to lie along one line in the plane of the sky, but this assumption will be relaxed later. The presence of the denser star–forming

core (referred to as simply "the core" from hereon) on the south–western edge complicates the radiative transfer, and models with and without this high density region are presented.

3.1. 2-D and 3-D models without the core

Fig. 2 presents the results of inhomogeneous models for the abundances of C and ^{12}CO with varying F and $\ell_{\rm cl}$. The adopted average density is $< n_{\rm H} >= 1000$ cm^{-3} with $R_{\rm ic}$ = 10, so that n_c = 3000 cm^{-3} and n_{ic} = 300 cm^{-3} for F = 25%. The average density is not well constrained by observations, but the adopted value is close to $< n_{\rm H} >= 600 - 1600$ cm^{-3} derived from the total ^{13}CO column density divided by the size of the cloud (Blair et al. 1978; Plume et al. 1994). The clump size $\ell_{\rm cl}$ is varied between 0.2 pc and 0.6 pc (0.7′ and 2.1′) and the volume filling factor F from 10% to 100%, keeping $< n_{\rm H} >= 1000$ cm^{-3}. For $\ell_{\rm cl}$=0.2 pc, the grid size is taken to be 500 × 500, corresponding to a resolution of 0.02 pc.

Fig. 2 shows the C and ^{12}CO abundances as functions of projected distance on the sky along the cut indicated in Fig. 1a. This cut includes both clumps and interclump gas. It is seen that the neutral carbon is much more extended in the inhomogeneous models than in the corresponding homogeneous model, where the C abundance starts to drop already after 0.6 pc. This extent increases roughly with $1/F$ and $\ell_{\rm cl}$: ultraviolet radiation penetrates deeper into the model cloud if the effective surface area is lower. The CO and C profiles are stratified, but they overlap on the surfaces of those clumps which are located $\geq$ 1 pc into the cloud. The intensities of [CI] 609 μm and the ^{13}CO 2-1 line for a three-dimensional model with F = 40% and $\ell_{\rm cl}$ = 0.4 pc are also indicated and correspond to an integration into the cloud for every point along the cut in Fig. 1a. These computations were performed on a 120 × 120 × 120 grid with the small chemical network. The abundance of ^{13}CO was obtained by simply scaling the ^{12}CO abundance by a factor of 60, since ^{13}C is not explicitly in the small chemical network. This approach may overestimate the ^{13}CO intensity by up to a factor of ∼2 at the edge of the cloud or clumps where isotope selective photodissociation plays a role. It is further assumed here that the ^{13}CO 2-1 line is optically thin. In Sect. 3.2 the interface region of the dense core will be incorporated as well. Species like C$^+$ and O mostly reside in the lower density gas. The former because neutral carbon is ionized by the interclump radiation field. The latter because CO does not self-shield in the interclump medium and can only bind a small fraction of the oxygen in the cloud. Their abundances remain high deeper into the cloud for lower values of F.

The dependence on filling factor and clump size is illustrated in more detail in Table 1, which shows the extent of the [CI] emission, $L_{\rm C}$, for a set of inhomogeneous models with $< n_{\rm H} >=$ 1000 cm^{-3}. The length scale $L_{\rm C}$ is defined as that region in the cloud over which the neutral carbon emission is present at a level of 25% or more of the peak emission found near the edge. The data of Plume et al. indicate that $L_{\rm C}$ is at least 2 pc. The results of Table 1 are shown graphically in Fig. 3 where $L_{\rm C}$ is plotted versus F for different values of the clump

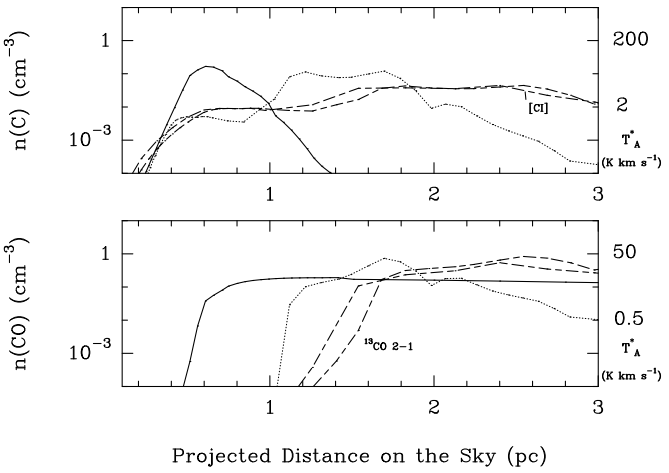

Fig. 2. Inhomogeneous models with $< n_H >$=1000 cm^{-3} and varying values of F and $\ell_{\rm cl}$. Dotted curve: $\ell_{\rm cl}$ = 0.2 pc and F = 60%, dashed curve: $\ell_{\rm cl}$ = 0.4 pc, F=40%. For the latter model, the ^{13}CO 2-1 and [CI] 609 μm intensities are presented as well. These were obtained by integrating into the cloud for every point along the cut in Fig. 1a. The homogeneous model is indicated by the solid line.

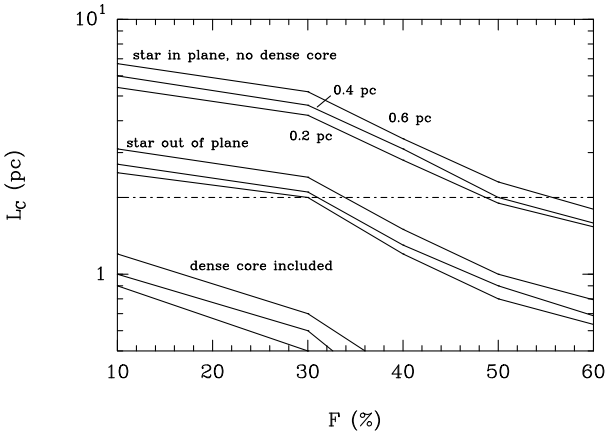

Fig. 3. The dependence of $L_{\rm C}$ on the volume filling factor for the models of Table 1. For each model, the clump size is 0.2, 0.4 and 0.6 pc for the lower, middle and upper curve, respectively. The dashed line indicates the observed carbon length scale by Plume et al. (1994).

size and various models. The dashed line indicates the Plume et al. results. It is seen that $L_{\rm C}$ increases significantly when F drops below 50%, but that the sensitivity to $\ell_{\rm cl}$ is not large. However, if these clumps become too small, $A_V < 1$ mag or $\ell_{\rm cl} < 0.2$ pc for F = 30%, the CO abundance does not become large enough to self–shield so that carbon stays mostly in atomic form. These effects are illustrated in the last column of Table 1 which presents the C and ^{13}CO column densities through a single clump of size $\ell_{\rm cl}$ for different values of F, corresponding to densities n_h ranging from 10^3 to 5×10^3 cm^{-3}. In order to simulate the average radiation field incident on such a clump in the extended cloud, I_{UV}=10 is used for a plane-parallel radiation field. It is apparent that the ^{13}CO column density decreases non-

Table 1. Carbon emission length scales[a] and column densities[d] of C and ^{13}CO

F(%)	$\ell_{\rm cl}$(pc)	$L_{\rm C}$(pc)	$L_{\rm C}$(pc)[b]	$L_{\rm C}$(pc)[c]	N(C)[d]	N(^{13}CO)[d]
100	0.2	0.5	0.1	0.3	7.9(14)	5.0(10)
80	0.2	1.0	0.1	0.4	2.0(15)	5.4(11)
50	0.2	1.9	0.2	0.8	3.1(15)	6.9(12)
40	0.2	2.8	0.3	1.2	5.8(15)	1.8(13)
30	0.2	4.2	0.5	2.0	9.4(15)	6.1(13)
10	0.2	5.4	0.9	2.5	5.1(16)	1.0(15)
100	0.4	0.5	0.1	0.3	3.0(15)	4.3(11)
80	0.4	1.0	0.1	0.4	5.2(15)	1.4(12)
50	0.4	2.0	0.2	0.9	1.3(16)	1.5(13)
40	0.4	3.1	0.3	1.3	2.8(16)	7.1(13)
30	0.4	4.6	0.6	2.1	4.9(16)	5.2(14)
10	0.4	6.0	1.0	2.7	2.2(17)	1.9(16)
100	0.6	0.5	0.1	0.3	8.9(15)	5.8(12)
80	0.6	1.1	0.2	0.5	1.3(16)	1.5(13)
50	0.6	2.3	0.3	1.0	5.0(16)	2.4(14)
40	0.6	3.4	0.4	1.5	7.4(16)	7.7(14)
30	0.6	5.2	0.7	2.4	1.1(17)	3.2(15)
10	0.6	6.7	1.2	3.1	3.0(17)	7.3(16)

[a] Defined as the size of the region within 25% of peak.
[b] Dense core included.
[c] Star out of the plane of the cloud.
[d] Column density in cm^{-2} through a clump with $< n_{\rm H} >= Fn_h + (1-F)n_l$ = 1000 cm^{-3} and $I_{\rm UV}$ = 10.

linearly for high values of F (low clump densities) and low $\ell_{\rm cl}$: even a superposition of such clumps would not give the observed ^{13}CO column densities of a few 10^{15} – 10^{16} cm^{-2}. For example, for F = 30%, there are typically 10-15 clumps along a line of sight in our model. The column density of neutral carbon also decreases with increasing F, but less strongly. Thus, in order to reproduce the observed correlation between C and ^{13}CO, the clumps need to be larger than 0.2 pc (45″) in size. High resolution ^{13}CO maps could provide a direct determination of this clump size.

Measuring the extent of the [CI] emission blobs directly does not lead to a good measure of the clump size, since some [CI] also originates in the interclump medium and since the integration along the line of sight of a number of (limb-brightened) clumps is difficult to deconvolve. The computed [CI] integrated antenna temperatures in the three-dimensional model, as shown in Fig. 2, are typically 10 K km s^{-1} at the edge and consistent with the observations.

In summary, it is concluded that for this geometry and adopted average density $< n_{\rm H} >= 1000$ cm^{-3}, F needs to be smaller than 40% and $\ell_{\rm cl}$ greater than 0.2 pc to reproduce the observed extent and magnitude of the [CI] emission and, although only partially, the correlation with ^{13}CO found by Plume et al. (1994).

3.1.1. 2-D models with the core

Observations show a dense, star–forming region located in projection close to the south–western edge of the cloud. Since this dense core lies directly along the line of sight from the illuminating star to the extended cloud, it can influence the penetration of photons considerably. In the second set of models, we have therefore included this region, which spans a solid angle of approximately 0.5 steradians for a spherical geometry. The average density over a region 0.5 pc in extent is $\approx 10^4$ cm^{-3} or $A_V \approx 10$ mag (Hayashi et al. 1985; Zhou et al. 1994). The adopted parameters for this core are $< n_{\rm H} >= 7 \times 10^3$ cm^{-3} with $R_{\rm ic}$ = 10. The typical size of the grid for the core region is 250×250. The physical grid-cell size is approximately an order of magnitude smaller than for the extended molecular cloud due to the higher density. The radiative transfer solution constructed in the core grid is used as a boundary condition for the extended molecular cloud.

The fourth column in Table 1 shows the same set of models, but with the dense core included. The filling factor of the clumps in the dense core is taken to be the same as that for the corresponding extended cloud model, whereas the size of a clump is chosen such that the clump has the same visual extinction. Because of the higher density in the core, the clumps are correspondingly smaller than in the extended cloud. It is clear from Table 1 that the extent of the [CI] emission in the molecular cloud cannot be reproduced by any model, even if F is as low as 10%. As shown in Sect. 4, this model does, however, reproduce the extent of the [CI] emission and the CO morphology for the interface region itself.

3.1.2. 3-D models with the star closer to the Sun

Since the dense core is obviously present, the star was moved closer to the sun to allow direct illumination of the surface of the molecular cloud facing the observer. The angle α between the line through the center of the molecular cloud and the dense core and the line between the center of the molecular cloud and the star is assumed equal to 10°. This puts the illuminating star 1.1 pc closer to the earth. This configuration is depicted in Fig. 1b. Because the angle through which the star is moved is only 10 degrees and 1.1 pc is comparable to the physical size of the dense core and much smaller than the total extent of the molecular, the sharp HII interface (radio continuum-Hα) is not expected to widen much.

The same combination of molecular cloud and core grid is chosen as for the two-dimensional models discussed above to solve the chemical and thermal balance. The continuum radiative transfer is solved in three dimensions on a $180 \times 180 \times 180$ grid. The effective enhancement of the radiation field is approximately 110 at the surface of the molecular cloud toward the dense core. The strength of the radiation field drops by factor of 6 toward the surface of the molecular cloud facing the observer. It has been verified that small changes in angle ($\alpha = 5 - 20°$) do not influence the qualitative or quantitative nature of our conclusions.

Fig. 4 shows the density and the corresponding [CI] 609 μm (grey scale), [CII] 158 μm (grey scale), ^{13}CO 2–1 (contours) and [OI] 63 μm (contours) maps for the model with $< n_{\rm H} >= 1000$ cm^{-3}, F = 30% and $\ell_{\rm cl}$ = 0.4 pc. For the core, $< n_{\rm H} >= 7 \times 10^3$

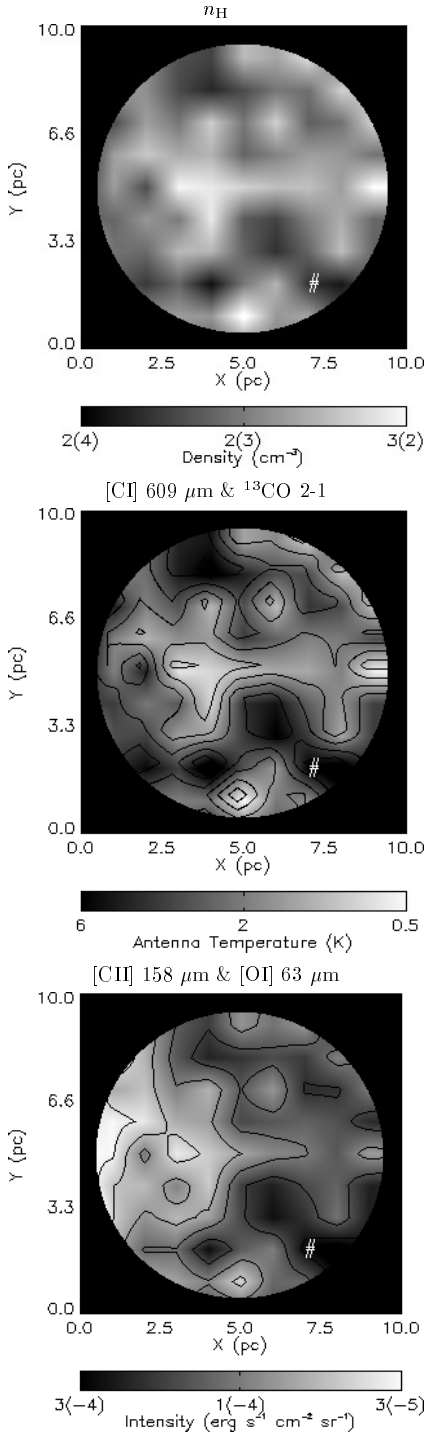

Fig. 4. Upper panel: density on the surface of the extended molecular cloud; middle panel: [CI] 609 μm (grey scale) and ^{13}CO 2–1 (contours) maps; lower panel: [CII] 158 μm (grey scale) and [OI] 63 μm (contours) maps for the generic model with $< n_{\rm H} >= 1000$ cm^{-3}, F = 30% and $\ell_{\rm cl}$ = 0.4 pc with the illuminating star 1.1 pc closer to the sun. The ^{13}CO contour levels run from 3 to 9 K in steps of 1 K. The [OI] 63 μm contour levels run from 5×10^{-6} to 5×10^{-5} erg s^{-1} cm^{-2} sr^{-1} in steps of 2×10^{-6} erg s^{-1} cm^{-2} sr^{-1}. The external star HD 211880 is located to the lower right of the figure. The dense core is located at the edge of the cloud to the lower right of the figure and is indicated by a #.

cm^{-3}, F = 30% and $\ell_{\rm cl}$ = 0.04 pc. The ^{13}CO values were again obtained by scaling the ^{12}CO abundances by a factor of 60. The correspondence in morphology between the [CI] and ^{13}CO 2–1 emission is striking and is a result of the angle between the star and the core, which creates a partial face-on appearance. The extent of the carbon emission is less than in the edge-on models without the dense core due to the decreased ultraviolet flux, but the morphology and the maps presented in Plume et al. (1994) are well reproduced, as is the magnitude of the line intensity. The constraint $\ell_{\rm cl} > 0.2$ pc (45″) still holds, and is observationally testable through ^{13}CO observations. The condition on F is now $F \leq$30%. With the star closer to the sun, variations in column density can also create a clumpy morphology. In fact, if the molecular cloud is homogeneous and is illuminated by the average interstellar radiation field enhanced by a factor of a few from both sides, then the total column and extent of atomic carbon can also be reproduced. Still, such a model has a relatively low density ($n_{\rm H} \approx 1000$ cm^{-3}) and temperature for the molecular material, and cannot reproduce the high column density necessary for the ^{13}CO line unless a density close to 4×10^3 cm^{-3} is adopted. If the inhomogeneous structures turn out to have smaller subcondensations, the density of these structures should be proportionally higher than the value of ∼3000 cm^{-3} for F = 30% adopted here for the formation of ^{12}CO and ^{13}CO to occur. Observations of high density tracers like HCO$^+$ and CS can provide upper limits on the clump densities.

The [CII] and [OI] brightness maps presented in Fig. 4 correlate well with each other since both lines have high excitation temperatures. The core is the dominant feature in the map and is indicated by a #. Although the low density interclump medium attains higher temperatures (∼ 250 K) than the clumps (∼ 100 K) away from the interface region, the density is (much) below the critical density of the lines and a rather tight correlation with the high density regions obtains.

3.2. Comparison with other work

Comparison of our detailed radiative transfer models with observations indicates that clump sizes of at least 0.2 pc and filling factors less than 30% are needed to reproduce the observed [CI] and CO emission in S 140. How do these results compare with those of others? Howe et al. (1991) used observations of [C II] 158 μm emission to determine the properties of the inhomogeneous medium. They define a length scale $L_{\rm C^+} \equiv \ell_{\rm cl}/F$, but in their formalism $\ell_{\rm cl}$ and F cannot be determined independently: to derive a clump volume filling factor F, a characteristic clump size must be chosen. For a clump size of 0.1 pc, they infer volume filling factors of 20–40% for PDRs such as NGC 1977 and NGC 2023, similar to our values for S 140. As shown by Spaans (1996), however, the [C II] emission arises mostly from the interclump medium, unless the interclump density is much lower than the critical density. Therefore, these types of measurements do not provide strong constraints on the clump size, only on the transparency of the interclump medium. Nevertheless, an additional conclusion from their work is that the density contrast between the clump and interclump gas must be

large, of order 100 for W3 and NGC 1977. In fact, they require an interclump density of $300 - 500$ cm^{-3}, corresponding to $A_{\rm V} \approx 0.5 - 0.75$ mag pc^{-1}, comparable to that adopted here for the S 140 molecular cloud. For these values the ultraviolet radiation is not redistributed in angle until it has traversed a distance of a few pc in the cloud, and thus stays high. Conversely, to reproduce the intensity and excitation of the [CII] 158 μm line they need clump densities of $\sim 10^5$ cm^{-3}. The combination of these two requirements drives their high value of $R_{\rm ic}$. The [CII] line intensity in S 140 is a factor of 5 lower than in W3 and NGC 1977: 4.6×10^{-4} versus 2.2×10^{-3} and 2.5×10^{-3} erg s^{-1} cm^{-2} sr^{-1}, respectively (Boreiko et al. 1990, Howe et al. 1991). Consequently, S 140 can be modeled with a lower value of $R_{\rm ic}$. Since it is likely that a range in clump densities exists, the best value of $R_{\rm ic}$ will depend on the atomic or molecular line that is modeled.

We have used the method of Howe et al. to determine the clump volume filling factors from the [C II] data discussed above with the clump sizes as given in Sect. 3.4 and compared them to our own results. The inferred filling factors generally agree well for their model 2/I (opaque clumps in a low–opacity scattering interclump medium). For their model 2/II (no scattering of ultraviolet photons in the interclump medium), however, the resulting values for F are not consistent with ours and the resulting [CII] line intensities for the F–values in Table 1 are systematically too low.

Finally, as noted in Sect. 3.3, a homogeneous cloud with $n_{\rm H} \approx 4 \times 10^3$ cm^{-3} illuminated isotropically by the average interstellar radiation field emits bright enough [CI] 609 μm and ^{13}CO 2-1 emission. Therefore it is possible that an inhomogeneous medium (with the star closer to the sun) is not required. underlying However, a point-source of illumination like HD 211880 prevents [CI] limb-brightening which would occur for isotropic illumination of a homogeneous medium and is not observed. Also, variations in column density would be required to produce the structure seen in the Plume et al. data.

4. The interface region

The interface region between the S 140 HII region and the molecular cloud has been studied extensively through high resolution observations of various species, including [CI] and CO (White & Padman 1991; Minchin et al. 1993, 1994), and CS (Snell et al. 1984; Hayashi et al. 1985; Zhou et al. 1994). In this region, which is only a few arcmin (0.5 pc) in extent, several different components can be distinguished. First, it includes the dense star–forming core, which contains the group of three embedded young stars which can illuminate the S 140 region from within. The density associated with the core is as high as 10^6 cm^{-3} in the immediate vicinity of the stars, but decreases outwards as a power law (Zhou et al. 1994). Second, there is a powerful, dense outflow associated with the embedded young stellar objects, which is observed in high velocity atomic and molecular gas. Third, an "arc" component along the ionization front between the H II region and the dense core has been found (Zhou et al. 1994). The density in this region is uncertain, but is lower than in the core. The clump density in the interface region must be at least 10^4 cm^{-3} in order to explain the widespread CS emission.

The interface region has been modeled as a 2–D inhomogeneous cloud exposed to $I_{\rm UV}$=150 incident perpendicular to the ionization front. It has clumps of density $n_c = 2 \times 10^4$ cm^{-3} embedded in an interclump medium of density $n_{ic} = 2 \times 10^3$ cm^{-3}. The clump volume filling factor is taken to be $F = 30$ %, based on the results of Zhou et al. (1994), and $\ell_{\rm cl}$=0.04 pc. The adopted grid is 250×250. No density gradient has been assumed, nor is the outflow region included explicitly. However, the radiation produced by the embedded stars can readily be taken into account in our models. Unfortunately, the extinction associated with the cocoons in which they are embedded is uncertain. For the present investigation, we have therefore represented the three stars by a single source with $I_{\rm UV} \approx 10$ at the position of IRS1. This value was chosen to yield the best qualitative agreement with observations (see below). In these models, the center of the molecular cloud, the interface region or dense core, and the exciting star are assumed to lie along one line in the plane of the sky.

Fig. 5 shows a mosaic for the adopted density field (upper left) and the resulting abundances of C$^+$ (middle right), C (lower right), CO (middle left) and ^{13}CO (lower left), together with the temperature structure (upper right). In the large network used for these calculations, the chemistry of ^{13}CO was computed explicitly. The atomic carbon is located predominantly at the surfaces of the clumps, whereas the C$^+$ is situated in the interclump medium. The extended nature of both the C$^+$ and C is evident from Fig. 5 and is caused by the enhanced penetration of ultraviolet photons. In the homogeneous model, the C$^+$ and C emission decreases sharply after 0.05 pc. In three dimensions the embedded sources create a spherical PDR. The temperature map in Fig. 5 also shows a warm region around the position of the embedded sources which are indicated by a *. The ionization fraction remains high ($> 2 \times 10^{-5}$) further into the cloud.

The extent of the [CI] emission and the effect of the embedded source is further illustrated in Fig. 6, which shows the ^{12}CO and C column densities as functions of offset with respect to the S 140 ionization front. The neutral carbon abundance increases rapidly from the HII region inward and turns over as the ^{12}CO column density reaches its (first) maximum, consistent with an edge-on PDR, resulting in the 'arc'–like structure. At the position of the embedded sources ($\sim 40''$ into the cloud) the ^{12}CO is dissociated and the C abundance is correspondingly increased. Further into the cloud ^{12}CO becomes the main sink for carbon once more. This structure agrees well with that observed by Minchin et al. (1994, their Fig. 8), both quantitatively and qualitatively. The best agreement with the data ($\sim$ a factor of two) is obtained for an internal source with $I_{\rm UV} = 10$. This number depends on the particular realization of the density field, but does not vary by more than a factor of two for $F = 30$ %.

Fig. 7 (solid curve) presents the temperature structure for a cut perpendicular to the ionization front (avoiding the embedded source) starting at a position at the edge, just inside the HII region, where the effective value of $I_{\rm UV} \approx 140$. The clumps

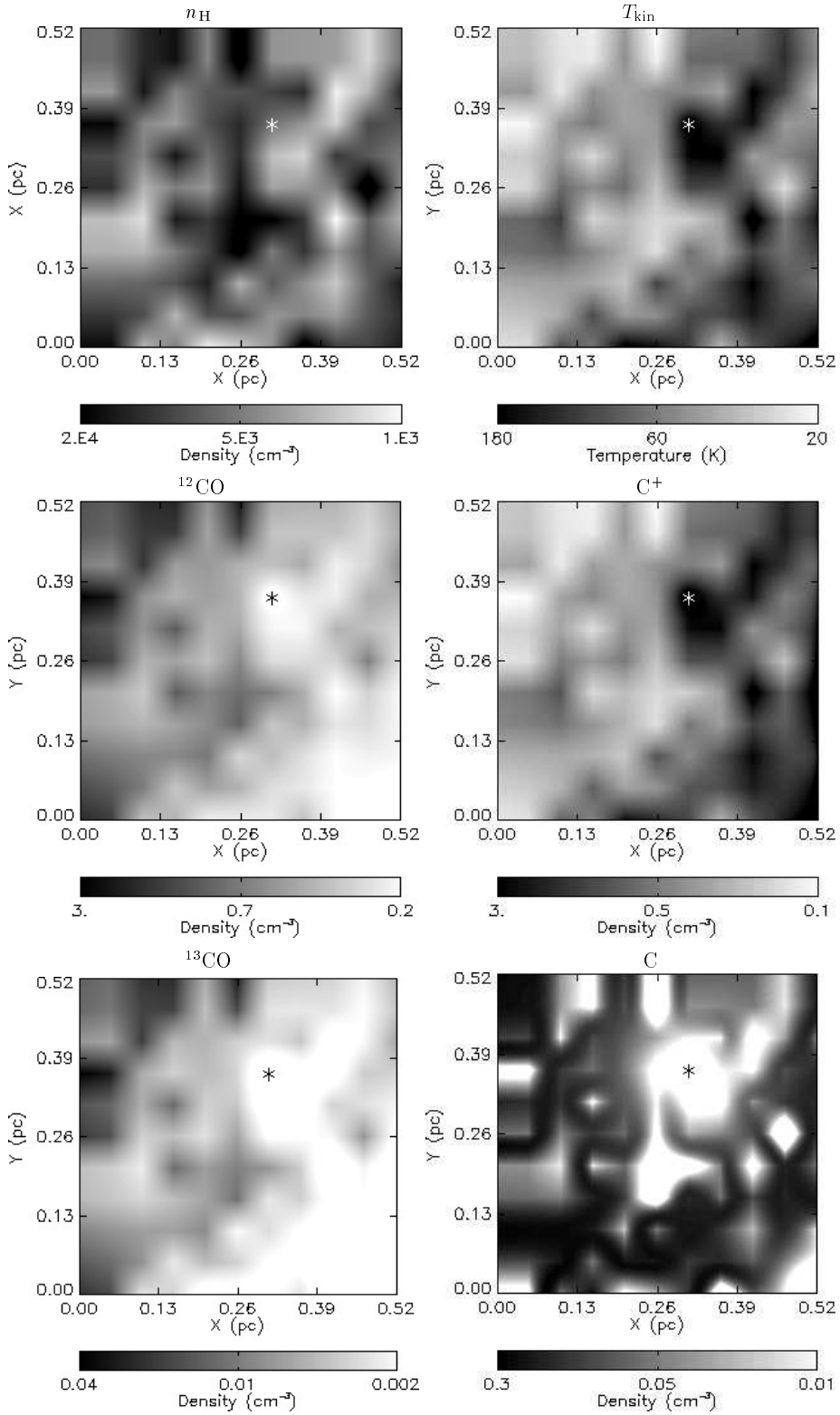

Fig. 5. Mosaic for the standard model of the interface region with n_c = 2 × 10^4 cm^{-3}, n_{ic} = 2 × 10^3 cm^{-3}, F =30%, $I_{\rm UV}$ = 150 and $I^i_{\rm UV}$ = 10 for the embedded source. The external star is located to the lower right of the figure and the embedded source is indicated by a *.

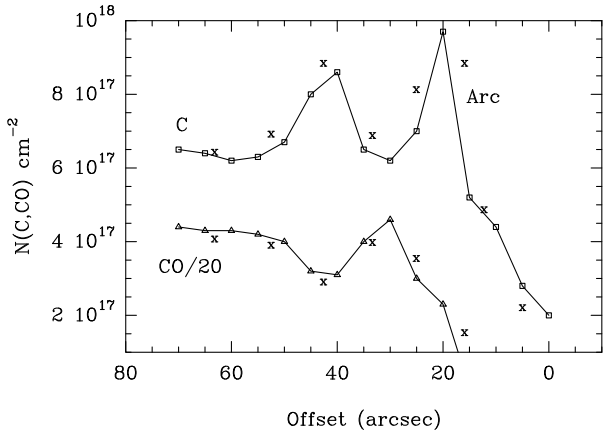

Fig. 6. Depth dependence of C and ^{12}CO column densities in the standard model. Crosses indicate the data of Minchin et al. (1994, their Fig. 8). The offset is with respect to the ionization front.

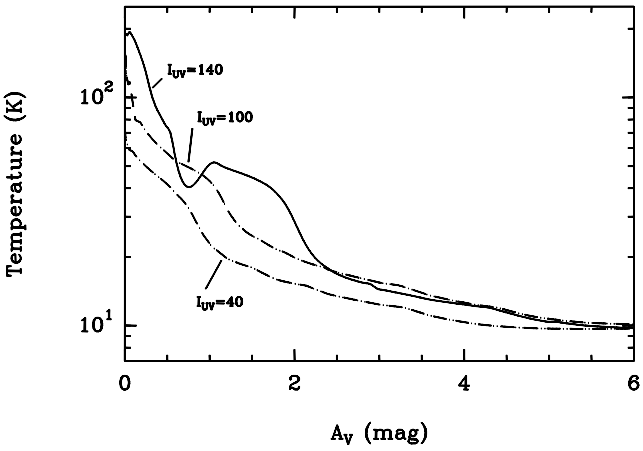

Fig. 7. One-dimensional temperature structure for the standard model of the interface region with n_c = 2 × 10^4 cm^{-3}, n_{ic} = 2 × 10^3 cm^{-3}, and F = 30%. Cuts perpendicular to the ionization front are presented for $I_{\rm UV} \approx 140$ (solid curve), $I_{\rm UV} \approx 100$ (upper dashed curve) and $I_{\rm UV} \approx 40$ (lower dashed curve) at the edge of the cloud.

only reach high ($T \approx 50 - 60$ K) temperatures at the edge of the cloud. For this model temperature differences between clump and interclump medium are of the order of 30-50 K for the first few magnitudes of extinction. The dashed curves in Fig. 7 present two additional cuts at $I_{\rm UV} \approx 100$ (upper dashed curve) and $I_{\rm UV} \approx 40$ for the interclump medium only. Geometrical dilution of the radiation field clearly causes a temperature gradient parallel to the ionization front. This effect should be directly observable through the brightness of the CO 6-5 line. For the illuminating star located closer to the sun this gradient is still present, but is less steep.

Recently, Timmermann et al. (1996) presented ISO SWS observations of pure rotational H_2 emission toward the interface region of S 140. These authors derive a kinetic temperature of approximately 500 K which is almost a factor of three higher than presented here. This discrepancy could be removed if the value of $I_{\rm UV}$ were underestimated by a factor of three to four. Although a factor of two higher value has been suggested by Timmermann et al. (1996), it is not clear where the additional radiation comes from. Alternatively, hydrodynamic effects in the interface region such as a weak shock may also heat the gas. A lower oxygen abundance will decrease the cooling rate if the [OI] fine-structure transitions are not very optically thick. Still, the [OI] 63 μm line is generally optically thick and likely to dominate at these temperatures and densities. Clearly, further research is warranted.

Fig. 8 shows the distribution of ^{12}CO rotational line emission at the position of the embedded sources and a position 25″ further south-east. The emission is generally brighter and more highly excited at the former position, since the young B stars produce a lot of warm molecular material, consistent with observations of Minchin et al. (1993).

In conclusion, the observed structure and extent of the [CI] and CO emission in the S 140 interface region can be well reproduced in an inhomogeneous model with $< n_{\rm H} >= 7 \times 10^3$ cm^{-3}, F = 30% and $\ell_{\rm cl}$ = 0.04 pc. The inhomogeneous structure and the inclusion of an embedded source of radiation are essential features of the model.

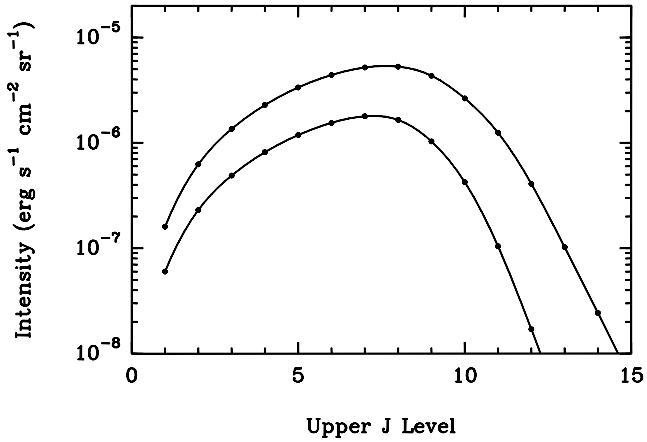

Fig. 8. Distribution of ^{12}CO rotational emission lines for the standard model at the position of the embedded sources (upper curve) and at a position 25″ further south-east.

5. Conclusions

Inhomogeneous models of the S 140 extended molecular cloud and interface region have been presented. The widespread [CI] emission in the molecular cloud is found to be well explained by an inhomogeneous sphere with $< n_H >= 10^3$ cm^{-3}, and a clump volume filling factor $F \leq 30\%$, illuminated by the star HD 211880. A minimum clump size $\ell_{\rm cl}$ = 0.2 pc is required to reproduce the tight correlation between [CI] and ^{13}CO line maps. Because of the presence of the dense star-forming core, the star must be located closer to the observer than the dense core to explain the [CI] extent. The [CI] emission observed in the

interface region is well explained by an inhomogeneous medium with $< n_{\rm H} >= 7 \times 10^3$ cm^{-3}, F = 30% and $\ell_{\rm cl}$ = 0.04 pc. In general, (partial) face-on illumination results in extended [CI] emission and structure present in the emission map can result from either clumps or simply variations in column density.

On a more general level, these investigations show that although one-dimensional homogeneous models of PDRs are well capable of reproducing many aspects of the observations, in some instances the intrinsic geometry of a source is essential and should be properly taken into account. The inclusion of inhomogeneous structure may be necessary in some cases to explain the widespread distribution of [CI] and [CII] emission and the correlation with ^{13}CO, but geometrical effects can play an equally large role. Especially the fact that the illuminating star does not necessarily lie along the line through the center of the molecular cloud and the dense core can result in a similar appearance.

Acknowledgements. The authors would like to thank David Jansen for stimulating discussions concerning interstellar chemistry. They are grateful to Dan Jaffe and Jocelyn Keene for critical comments on an earlier draft and for sending unpublished ^{12}CO and ^{13}CO maps of the region. The authors also thank the referee Jürgen Stutzki for his detailed and valuable suggestions. This work was supported in part by a PIONIER grant from the Netherlands Organization of Scientific Research (NWO) and for MS by NASA grant NAGW-3147 from the Long Term Space Astrophysics Research Program. Most of the simulations presented in this work were performed on the Cray Y-MP operated by the Netherlands Council for Supercomputer Facilities in Amsterdam.

References

Bakes E. L. O., Tielens A. G. G. M. 1994, ApJ 427, 822
Beichman C. A., Becklin E. E., Wynn-Williams C. G. 1979, ApJL 232, L47
Blair G. N., Evans N. J. II, Vanden Bout P. A., Peters W. L. III 1978, ApJ 219, 896
Boissé P., 1990, A&A 228, 483
Boreiko R. T., Betz A. L., Zmuidzinas J. 1990, ApJ 353, 181
Burton M. G., Hollenbach D. J., Tielens A. G. G. M. 1990, ApJ 365, 620
Cardelli J. A., Mathis J. S., Ebbets D. C., Savage B. D. 1993, ApJL 402, L17
Crampton D., Fisher W. A. 1974, Pub. Dom. Ap. Obs. 14, 12
Draine B. T., 1978, ApJS 36, 595
Evans N. J., III, Mundy L. G., Kutner M., DePoy D. L., 1989, ApJ 346, 212
Falgarone E., Pérault M. 1988, A&A 205, L1
Graf U. U., Genzel R., Harris A. I., Hills R. E., Russell A. P. G., 1990, ApJL 358, L49
Hayashi M., Hasegawa T., Gatley I., Garden R., Kaifu N., 1985, MNRAS 215, 31
Hernichel J., Krause D., Rörig R., Stutzki J., Winnewisser G. 1992, A&A 259, L77
Hogerheijde M. R., Jansen D. J, van Dishoeck E. F., 1995, A&A 294, 792
Hollenbach D. J., Takahashi T., Tielens A. G. G. M., 1991, ApJ 377, 192
Howe J. E., Jaffe D. T., Genzel R., Stacey G. J., 1991, ApJ 373, 158
Jansen D. J., van Dishoeck E. F., Black J. H., Spaans M., Sosin C., 1995a, A&A 302, 223
Jansen D.J., Spaans M., Hogerheijde M.R., van Dishoeck E.F., 1995b, A&A 303, 541
Jansen D. J., van Dishoeck E. F., Keene J., Boreiko R.T., Betz A.L., 1996, A&A 309, 899
Jaffe D.T., Zhou S., Howe J.E., Hermann F., Madden S.C. et al. 1994, ApJ 436, 203
Keene J., 1995, in "Proceedings of the 2nd Cologne-Zermatt Symposium", G. Winnewisser (ed.), p.186
Keene J., Blake G. A., Phillips T. G., Huggins P. J., Beichman C. A., 1985, ApJ 299, 967
Köster B., Störzer H., Stutzki J., Sternberg A., 1994, A&A 284, 545
le Bourlot J., Pineau des Forêts G., Roueff E., Flower D.R., 1993, A&A 267, 233
Luhman M.L., Jaffe D.T., Keller L.D., Pak S.J., 1994, ApJL 436, L185
Meixner M., Tielens A. G. G. M., 1993, ApJ 405, 216
Minchin N. R., White G. J., Padman R., 1993, A&A 277, 595
Minchin N. R., White G. J., Stutzki J., Krause D., 1994, A&A 291, 250
Plume R., Jaffe D. T., Keene J., 1994, ApJL 425, L49
Smith D., Spañel P., 1993, Chem. Phys. Lett. 211, 454
Snell R. L., Mundy L. G., Goldsmith P. F., Evans N. J., II, Erickson N. R., 1984, ApJ 276, 625
Spaans M., 1996, A&A 307, 271
Spaans M., Tielens A. G. G. M., van Dishoeck E. F., Bakes E. L. O., 1994, ApJ 437, 270
Sternberg A., 1986, Ph. D. Thesis, Columbia University
Stacey G. J., Jaffe D. T., Geis N., Genzel R., Herrman F., Jackson, J. et al., 1993, ApJ 404, 219
Stutzki J., Stacey G. J., Genzel R., Harris A. I., Jaffe D. T., Lugten J. B., 1988, ApJ 332, 379
Tauber J. A., Lis D. C., Keene J., Schilke P., Büttgenbach T. H., 1995, A&A 297, 567
Tielens A. G. G. M., Hollenbach D. J., 1985, ApJ 291, 722
Timmermann R., Bertoldi F., Wright C.M., Drapatz S., Draine B.T., Haser L., Sternberg A., 1996, A&A 315, L281
van Dishoeck E. F., Black J. H., 1988, ApJ 334, 771
White G. J., Padman R., 1991, Nature 354, 511
Yui Y. Y., Nakagawa T., Doi Y., Okuda H., Shibai H., Nishimura T., Low, F., 1993, ApJL 419, L37
Zhou S. D., Butner H. M., Evans N. J., Güsten R., Kutner M. L., Mundy L. G., 1994, ApJ 428, 219
Zhou S., Evans N. J., Mundy L. G., Kutner M. L., 1993, ApJ 417, 613

This article was processed by the author using Springer-Verlag LaTeX A&A style file *L-AA* version 3.